Dalton Transactions

ROYAL SOCIETY OF CHEMISTRY

PAPER

View Article Online
View Journal | View Issue

Cite this: *Dalton Trans.*, 2024, **53**, 18021

Catalytic partial oxidation of methane over oxide-ion-conductive lanthanum silicate apatites†

Afif Pamungkas, [a] Yuta Goto,[a] Kazumasa Murata, [b] Saburo Hosokawa, [c] Satoshi Ogawa, [a] Kosaku Ohishi, [a] Tomohiro Matsumoto, [a] Miwa Saito [a] and Teruki Motohashi *[a]

Received 26th August 2024,
Accepted 18th October 2024

DOI: 10.1039/d4dt02421d

rsc.li/dalton

A lanthanum silicate $La_{9.33}Si_6O_{26}$ (LSO) crystallizes in an apatite-type structure and has been known as a promising oxide-ion conductor. Here, we report the activity of LSO for catalytic partial oxidation of methane (CPOX) to synthesis gas. The LSO catalyst demonstrated relatively high catalytic activity from 500 to 700 °C, with CH_4 conversion reaching 22.1% at 700 °C while retaining moderate CO and H_2 selectivities of 20–60%. Notably, LSO exhibited higher CPOX activity than non-apatite-type La_2SiO_5 despite their similar specific surface areas. The higher CPOX activity of LSO is likely attributed to its structural superiority involving mobile oxide ions in the crystal structure. The reaction kinetic study showed that the reaction orders for methane and oxygen in the CPOX reaction over the LSO catalyst were 0.69–0.73 and 0.08–0.21, respectively. Furthermore, the small contribution of adsorbed O species generated from gas-phase O_2 molecules indicated that the lattice oxygen may be involved in the reaction mechanism. The kinetic isotope effect (KIE) study using a CD_4 suggested that C–H bond breaking is the rate-determining step of CPOX over LSO.

Introduction

Methane is the primary component of natural gas and a vital carbon feedstock due to its abundance. However, converting methane into value-added chemicals, such as methanol and ethylene, is challenging because of its high stability and the complexity of multistep reactions. This challenge has driven research on selective methane oxidation. One approach to selective methane conversion is a direct route that yields products from methane in a single step. Alternatively, an indirect process converts methane into syngas, an intermediate raw material, which offers several advantages. Syngas, composed of CO and H_2, is industrially significant as a precursor for synthesizing valuable chemicals such as acetic acid and methanol.[1] Furthermore, syngas production is more energy-efficient than direct routes, which typically suffer from low yield problems.[2]

Various processes to produce syngas include dry reforming of methane (DRM) (1), steam reforming of methane (SRM) (2), catalytic partial oxidation of methane (CPOX) (3), and autothermal reforming of methane (ATR) (4), which combines SRM and CPOX. Among these, CPOX potentially offers notable benefits. It requires less energy input owing to its exothermic nature, in contrast to the endothermic processes of DRM and SRM. Furthermore, this reaction produces syngas with an H_2 to CO ratio of 2 : 1, which is optimal for methanol synthesis.

$$CH_4 + CO_2 \rightarrow 2CO + 2H_2 \quad (1)$$

$$CH_4 + H_2O \rightarrow CO + 3H_2 \quad (2)$$

$$CH_4 + \frac{1}{2}O_2 \rightarrow CO + 2H_2 \quad (3)$$

$$CH_4 + x/2O_2 + (1-x)H_2O \rightarrow CO + (3-x)H_2 \quad (4)$$

Catalytic oxidation reactions generally involve an oxygen transfer step, where the oxygen species migrates from the catalyst surface to the reactant. To ensure the smooth process of oxygen transfer, oxygen mobility on catalysts is important due to its impact on reactivity. High oxygen mobility allows for fast surface diffusion and absorption into the subsurface, thereby affecting the reaction rate.[3] Moreover, catalysts with oxide-ion conductive capability can supply active oxygen species to active sites, further enhancing catalytic activity.[4]

[a]*Department of Applied Chemistry, Faculty of Chemistry and Biochemistry, Kanagawa University, Yokohama 221-8686, Japan. E-mail: t-mot@kanagawa-u.ac.jp*
[b]*Mitsubishi Chemical Corporation, 1000 Kamoshida-cho, Aoba-ku, Yokohama 227-8502, Japan*
[c]*Faculty of Materials Science and Engineering, Kyoto Institute of Technology, Kyoto 606-8585, Japan*

† Electronic supplementary information (ESI) available. See DOI: https://doi.org/10.1039/d4dt02421d

Previous research has shown that high oxide ion mobility in the catalyst correlates with faster oxygen transfer, thereby influencing the reaction rate. For example, Zhu *et al.* demonstrated that Y-doped ZrO_2 facilitates a faster CPOX reaction than pure ZrO_2 because of the enhanced oxygen diffusion.[5] In the study on *n*-butene oxidative dehydrogenation over γ-Bi_2MoO_6, Jung *et al.* observed that catalytic performance is closely related to the oxygen mobility of the catalyst.[6] Yan *et al.* investigated the oxidative dehydrogenation of 1-butene with CO_2 over $Fe_2O_3/\gamma Al_2O_3$ catalyst and found that the catalytic activity increases linearly with oxygen mobility.[7] Borchert *et al.* reported that increased oxygen conductivity improves the C_2 selectivity during the oxidative coupling of methane (OCM) over metal oxide-doped La_2O_3.[8] Whereas OCM does not involve the oxygen species migration to the reactant (CH_4), the conductivity would still benefit OCM by enhancing oxygen adsorption and its transformation into lattice oxygen. Furthermore, it was found that oxygen-conducting catalysts ($Pt/(Ce_{0.71}Gd_{0.29})O_{2-x}$) suppress carbon deposit formation more effectively compared to non-oxygen conducting catalysts ($Pt/\gamma Al_2O_3$).[9]

Motivated by these findings, we conducted screening tests for CPOX activity on various compounds exhibiting oxide ion conductivity capabilities. Notably, high CPOX activity was discovered in a lanthanum silicate $La_{9.33}Si_6O_{26}$, hereafter denoted as "LSO", which possesses an apatite-type structure. Many research groups have previously focused on the ionic conductive capability of LSO.[10–14] Nevertheless, to our knowledge, no studies have dealt with the CPOX catalytic activity of LSO. Here, we report the CPOX activity of the LSO catalyst, demonstrating its high selectivity for syngas and superior catalytic activity compared to a non-apatite-type lanthanum silicate.

Experimental

Catalyst preparation

The compounds investigated in this study were synthesized using a solid-state reaction method. The target chemical compositions, starting reagents used, and synthesis conditions for these compounds are summarized in Table S1 of the ESI.† Polycrystalline samples of LSO and its substituted derivatives were also prepared. The phase purity of the resultant samples was verified using X-ray powder diffraction (XRD; Rigaku Ultima IV) with Cu-Kα radiation. Nitrogen gas adsorption/desorption isotherms were measured at 77 K (Microtrac BEL, BELSORP-mini II), and the specific surface area was calculated using the Bruauer–Emmett–Teller (BET) method.

Catalytic activity tests

A 50 mg catalyst was loaded into a quartz tube (inner diameter ≈ 0.5 cm) and supported by quartz wool on both sides. The tube, with both ends connected to a gas line, was positioned inside a tubular furnace. A gas mixture containing CH_4 (2.5 mL min^{-1}), O_2 (1.25 mL min^{-1}), and N_2 (6.25 mL min^{-1}) was passed through the catalyst before the temperatures were raised. The effluent gas was analyzed using a gas chromatograph (GC-TCD; INFICON Micro GC Fusion) connected to the gas line outlet. The conversion, yield, and selectivity were calculated using the following formulas, where *X*, *Y*, and *S* represent conversion, yield, and selectivity, respectively.

$$X_{CH_4} = \frac{n_{CH_4\,in} - n_{CH_4\,out}}{n_{CH_4\,in}} \times 100\% \quad (5)$$

$$Y_{CO} = \frac{n_{CO}}{n_{CH_4\,in}} \times 100\% \quad (6)$$

$$Y_{H_2} = \frac{n_{H_2}}{2 \times n_{CH_4\,in}} \times 100\% \quad (7)$$

$$S_{CO} = \frac{Y_{CO}}{X_{CH_4}} \times 100\% \quad (8)$$

$$S_{H_2} = \frac{Y_{H_2}}{X_{CH_4}} \times 100\% \quad (9)$$

The kinetic isotope effect (KIE) was investigated using equipment similar to that employed for the conventional catalytic activity tests. The catalytic activity of a 100 mg catalyst was measured with a gas mixture containing either normal methane or deuterated methane (CH_4 or CD_4, 5 mL min^{-1}), O_2 (2.5 mL min^{-1}), and N_2 (12.5 mL min^{-1}). The KIE value was calculated from the ratio of the CH_4 oxidation rate to the CD_4 oxidation rate.

Results and discussion

Screening tests for CPOX activity

The compounds tested as CPOX catalysts include perovskite-type $La_{0.8}Sr_{0.2}Ga_{0.8}Mg_{0.2}O_{2.55}$ (LSGM), brownmillerite-type $Ba_2In_2O_5$ (BIO), fluorite-type $Bi_{1.4}Y_{0.6}O_3$ (BYO), pyrochlore-type $Y_2Ti_2O_7$ (YTO), and melilite-type $LaCaAl_3O_7$ (LCA). As demonstrated in Fig. 1, the CPOX activity appears to depend strongly on the chemical composition and/or crystal structure of the catalysts. LSGM and LCA exhibit relatively high conversion and CO selectivity. Similarly, YTO displays high conversion but low selectivity. We also discovered high CPOX activity in the apatite-type $La_{9.33}Si_6O_{26}$ (LSO). Fig. 2a presents a schematic illustration of the LSO crystal structure.[15,16] Apatites with the general formula of $A_{10-x}(BO_4)_6X_y$ typically belong to the $P6_3/m$ (176) space group within a hexagonal system. In this formula, "*A*" represents cations such as Na, Ca, La, *etc.*; the BO_4 tetrahedral group includes SiO_4^{4-}, PO_4^{3-}, *etc.*; and "*X*" denotes anions, including O^{2-}, OH^-, F^-, *etc.*[17] The anions "*X*" occupy channels along the *c*-axis and exhibit high mobility, which is responsible for the unique ionic conductivity of apatites.

Catalyst characterization of LSO

XRD analysis indicates that the diffraction pattern for the LSO sample is essentially identical to that previously reported for apatite-type $La_{9.33}Si_6O_{26}$ [18] (Fig. 3). The lattice parameter values agree with those for the reference (Table S2†). No diffraction peaks from secondary phases are visible, demonstrating

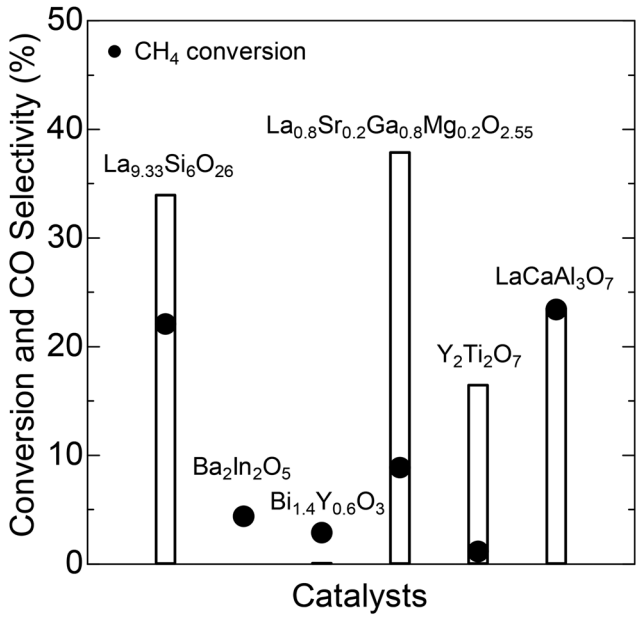

Fig. 1 CH_4 conversion and CO selectivity (at 700 °C) over various catalysts exhibiting oxide-ion-conductive capabilities.

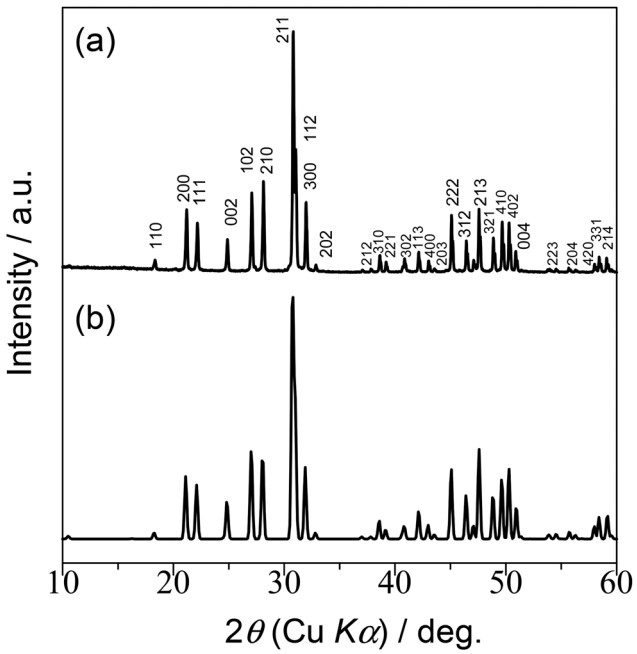

Fig. 3 XRD pattern of LSO from (a) this work and (b) ref. 18

the high quality of the sample. The specific surface area of the sample is estimated to be 0.32 $m^2\ g^{-1}$. The low value of the surface area is indicative of the presence of coarse grains with high crystallinity.

Catalytic activity of LSO

The LSO catalyst predominantly produces CO as the main carbon product at 500 and 600 °C (Fig. 4 and Table S3†). The CO selectivity exceeds 50% at these temperatures, with a downward trend at higher temperatures. Conversely, the CO_2 selectivity remains relatively constant at approximately 40% from 500 to 700 °C. Additionally, a small amount of C_2 hydrocarbons, likely resulting from OCM, is observed, with C_2 selectivity surpassing 20% at 700 °C. Hydrogen evolution exhibits a similar trend to that of CO, with the highest H_2 selectivity recorded at 39.2% at 500 °C, decreasing progressively to 19.2% at 700 °C due to the successive oxidation to water at elevated temperatures. The long-term catalytic test was conducted on LSO at 700 °C for 72 h. As demonstrated in Fig. S1,† LSO exhibits stable conversion and syngas selectivity throughout the reac-

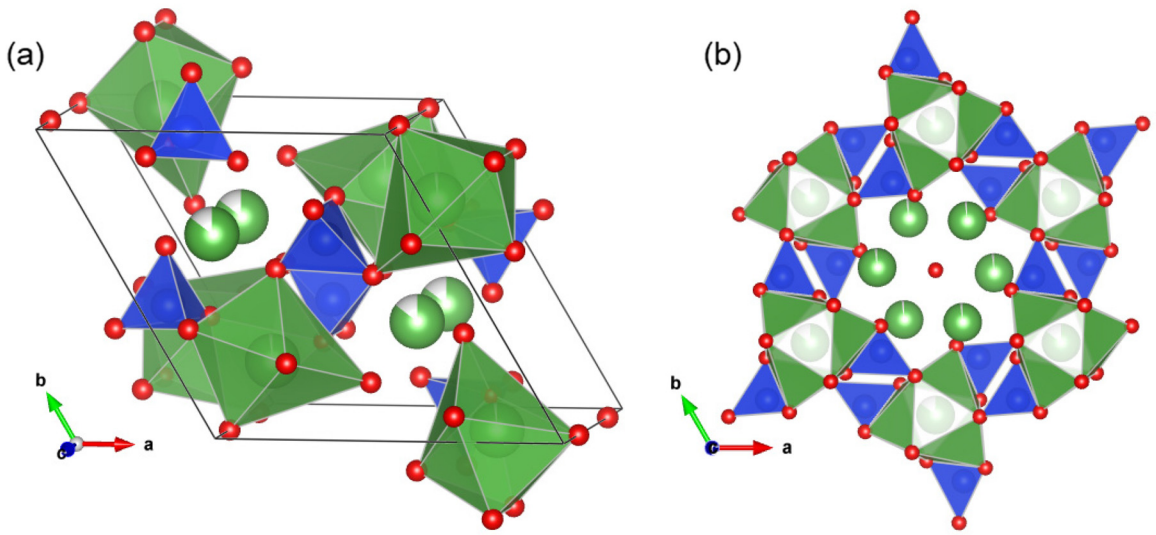

Fig. 2 (a) Schematic representation of the $La_{9.33}Si_6O_{26}$ apatite structure drawn with VESTA software.[15] (b) La and Si polyhedra enclose a one-dimensional tunnel containing mobile oxide ions (a red sphere in the middle). Color coding: green = La, blue = Si, red = O. Crystallographic data were extracted from ref. 16

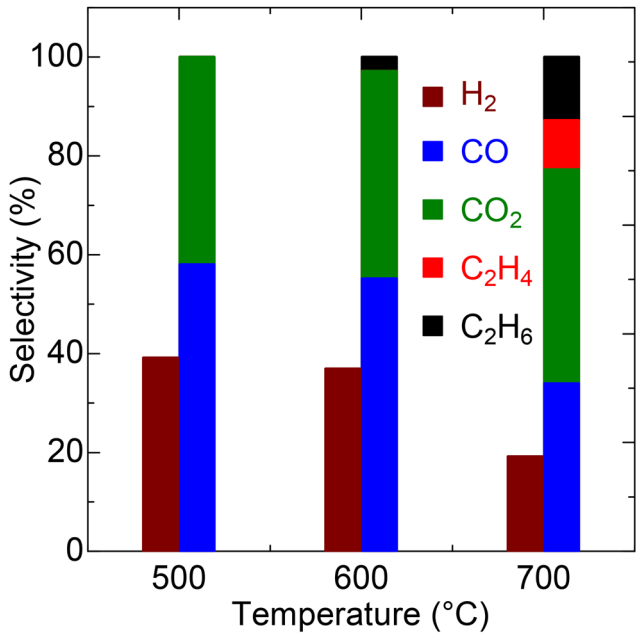

Fig. 4 Selectivity values for LSO in CPOX at different temperatures.

tion period. This result indicates that the catalyst maintains high stability during extended catalytic testing.

To discuss the crystallographic superiority of LSO on the CPOX performance, the catalytic activity was compared to that of La_2SiO_5, a non-apatite-type lanthanum silicate (Fig. S2 and Table S4†). As discussed in the previous section, LSO has mobile oxide ions in its structure (Fig. 2b). These anions are prone to oxide ion conduction and can promote catalytic oxidation.[19] Moreover, oxide ion conductivity facilitates oxygen supply and, consequently, enhances the reactivity.[20,21] Unlike LSO, La_2SiO_5 possesses a monoclinic structure[22] and does not contain mobile oxide ions. As presented in Fig. 5a, b and Table S3,† methane conversion over LSO is 22.1% at 700 °C; the CO and H_2 yields at this temperature are 7.5% and 4.2%, respectively. These values are higher than X_{CH_4} = 13.3%, Y_{CO} = 6.2, and Y_{H_2} = 3.1 for La_2SiO_5, as summarized in Table S5.† Although the specific surface area of LSO is slightly larger than that of the La_2SiO_5 sample (0.24 m^2 g^{-1}), the higher CH_4/O_2 conversions by a factor of ~2 cannot be solely attributed to differences in surface area. Further analysis reveals that the specific surface area of the catalyst is not a decisive factor for catalytic performance (see "Reaction kinetic study" section), suggesting that the enhanced activity of LSO is likely originating from its oxide ion conductivity.

The results of CPOX activity tests for chemically substituted LSO (Fig. S3†) further support our hypothesis. As demonstrated in Fig. S4,† sodium-substituted LSO ($La_9NaSi_6O_{26}$, LNSO) and calcium-substituted LSO ($La_8Ca_2Si_6O_{26}$, LCSO) exhibit significantly lower methane conversion than pristine LSO. Previous studies on oxide-ion conductive properties of chemically substituted LSO have reported that substituting Na and Ca at the La site reduces oxide-ion conductivity due to the decreased concentration of cation vacancies.[23,24] Considering the similar grain microstructures in LSO, LNSO, and LCSO, the substantially lower methane conversion activity of LNSO and LCSO can be attributed to their reduced oxide-ion mobility within the crystal structures. Notably, a favorable impact of oxide-ion conductivity (and thereby oxide-ion mobility) on oxidative catalytic activity has been suggested.[25,26] Jung *et al.* investigated the oxidative dehydrogenation reaction of *n*-butene to 1,3-butadiene over $Ni_9Fe_3Bi_1Mo_{12}O_{51}$ catalysts prepared under various pH conditions. They found that the catalyst prepared at pH 8 exhibited the highest oxygen mobility and catalytic activity.[27] Additionally, another study on the

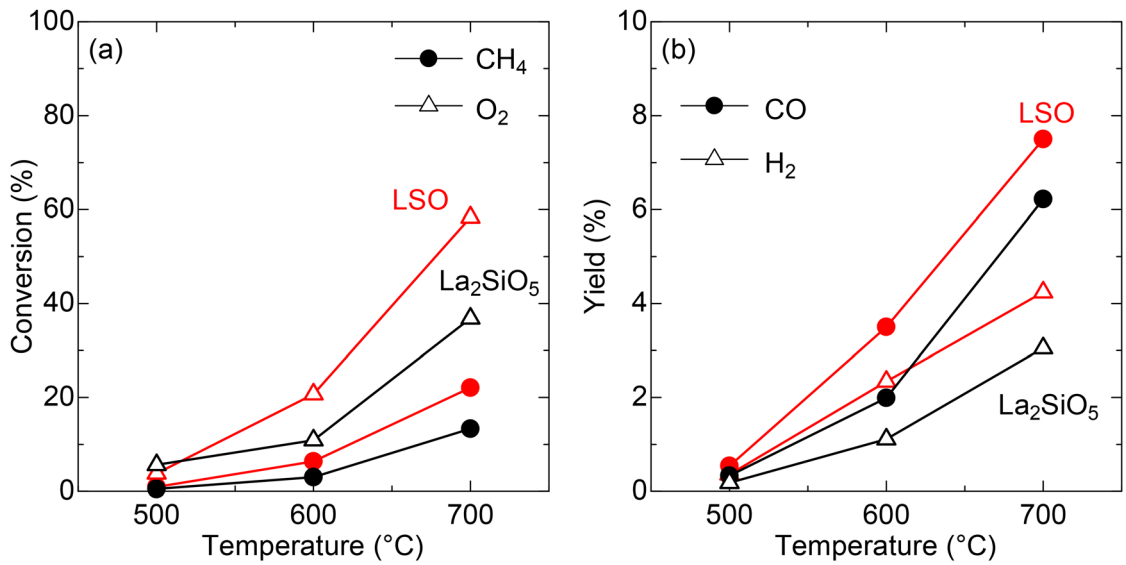

Fig. 5 (a) Catalytic conversions over LSO (red) and La_2SiO_5 (black). Circles and triangles denote values for CH_4 and O_2, respectively. (b) Catalytic yields over LSO (red) and La_2SiO_5 (black). Circles and triangles denote values for CO and H_2, respectively.

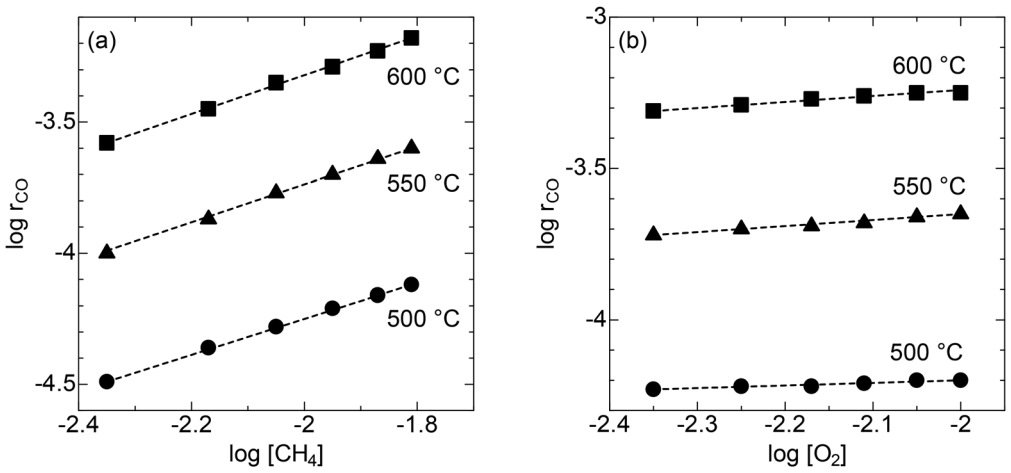

Fig. 6 Linear correlations between log r_{CO} and (a) log [CH_4] (O_2 concentration: 12.5%) and (b) log [O_2] (CH_4 concentration: 25%) at 500, 550, and 600 °C. The total flow rate is set at 10 mL min^{-1}.

same reaction revealed superior catalytic activity of multicomponent bismuth molybdate ($Co_9Fe_3Bi_1Mo_{12}O_{51}$) over pristine bismuth molybdate (γ-Bi_2MoO_6) due to the enhanced oxygen mobility of the former.[28]

Reaction kinetic study

The reaction kinetic study was performed to gain mechanistic insights into CPOX over the LSO catalyst. For CPOX reactions over oxide catalysts, the methane oxidation rate as a function of methane and oxygen partial pressures depends on the different oxygen species that activate methane.[29–33] The analysis focused on methane conversions of less than 10% to avoid heat and mass transfer issues.[34] Three different temperatures were chosen for this experiment: 500 °C, 550 °C, and 600 °C. The methane oxidation rate over LSO increases with increasing methane concentration (Fig. 6a). In contrast, the methane oxidation rate is nearly independent of oxygen concentration (Fig. 6b). From the reaction rate equation $r_{CH_4} = k[CH_4]^{\alpha}[O_2]^{\beta}$, the estimated reaction orders for methane and oxygen in the CPOX reaction are 0.69–0.73 and 0.08–0.21, respectively (Table 1). The reaction order of O_2 indicates that the contribution of adsorbed oxygen species on the surface, which are generated from gaseous O_2 molecules, is small in the CPOX reaction on LSO.[29,35] Considering the significant oxide-ion conductive capability of LSO, the results suggest that CPOX proceeds through the Mars–Van Krevelen mechanism, in which methane is oxidized by lattice oxygen. Additionally, the high reaction order for methane suggests that methane activation is the rate-determining step for methane oxidation on LSO.

Table 1 Summary of α, and β values at 500, 550, 600 °C

T/°C	α	β
500	0.69	0.08
550	0.73	0.21
600	0.73	0.19

The kinetic isotope effect (KIE) experiments were conducted using CD_4 to investigate a rate-determining step in the CPOX reaction over LSO. The KIE values are estimated to be 2.00 and 1.47 at 600 °C and 700 °C, respectively, from the ratio between the CH_4 and CD_4 oxidation rates. The KIE values larger than unity indicate that C–H bond breaking is the rate-determining step during the CPOX reaction over the LSO catalyst.[36] This finding is consistent with past research on CPOX catalysts.[37–39] Based on this finding, improving methane activation, for example, by adding transition metals, would further enhance the catalytic activity of LSO. Transition metals, such as nickel, can effectively facilitate the C–H bond breaking, thereby lowering the activation energy and increasing the reaction rate.[40]

Conclusion

To explore potential candidate materials for catalytic partial oxidation of methane (CPOX), the present work investigated the catalytic activity of $La_{9.33}Si_6O_{26}$ (LSO) with an apatite-type structure. The LSO catalyst demonstrated relatively high CPOX activity at temperatures from 500 to 700 °C, with CH_4 conversion reaching 22.1% at 700 °C and CO and H_2 selectivities of 34.0% and 19.2%, respectively. Notably, the CPOX activity of LSO is higher than that of La_2SiO_5 with a non-apatite-type structure despite their similar specific surface areas, highlighting the structural superiority of LSO containing mobile oxide ions in its crystal structure. The reaction kinetic study reveals that lattice oxygens in LSO contribute to the catalytic reaction. Furthermore, the kinetic isotope effect (KIE) study suggests that C–H bond breaking is the rate-determining step of CPOX over LSO.

Data availability

The data supporting this article have been included as part of the ESI.†

Conflicts of interest

There are no conflicts to declare.

Acknowledgements

This study was partly supported by JSPS KAKENHI Grant Number JP22H05143 (Transformative Research Area (A) "Supra-ceramics").

References

1 R. Detz, M. Beerse, N. Meulendijks, P. Buskens and B. van der Zwaan, *ChemSusChem*, 2024, e202400059.
2 L. Sun, Y. Wang, N. Guan and L. Li, *Energy Technol.*, 2020, **8**, 1900826.
3 M. E. Turano, E. A. Jamka, M. Z. Gillum, K. D. Gibson, R. G. Farber, W. Walkosz, S. J. Sibener, R. A. Rosenberg and D. R. Killelea, *J. Phys. Chem. Lett.*, 2021, **12**, 5844–5849.
4 N. Nunotani, *J. Ceram. Soc. Jpn.*, 2022, **130**, 825–831.
5 J. Zhu, J. G. van Ommen, H. J. M. Bouwmeester and L. Lefferts, *J. Catal.*, 2005, **233**, 434–441.
6 J. C. Jung, H. Kim, A. S. Choi, Y. M. Chung, T. J. Kim, S. J. Lee, S. H. Oh and I. K. Song, *Catal. Commun.*, 2007, **8**, 625–628.
7 B. Yan, L. Wang, B. Wang, F. Alam, Z. Xiao, J. Li and T. Jiang, *Appl. Catal., A*, 2019, **572**, 71–79.
8 H. Borchert and M. Baerns, *J. Catal.*, 1997, **168**, 315–320.
9 M. Salazar, D. A. Berry, T. H. Gardner, D. Shekhawat and D. Floyd, *Appl. Catal., A*, 2006, **310**, 54–60.
10 Y. Ogura, T. Yokoi, K. Fujii, M. Yashima and K. Matsunaga, *Solid State Ion.*, 2021, **373**, 115793.
11 C. A. Fuller, M. J. Gutmann, C. D. Ling, C. H. Wang, W. Zhang, P. S. Halasyamani, I. R. Evans and J. S. O. Evans, *J. Mater. Chem. A*, 2022, **10**, 14576–14584.
12 A. Mineshige, A. Saito, M. Kobayashi, H. Hayakawa, M. Momai, T. Yazawa, H. Yoshioka, M. Sakao, R. Mori, Y. Takayama, Y. Kagoshima and J. Matsui, *J. Power Sources*, 2020, **475**, 228543.
13 S. Okada, F. Maekawa, R. Tago, Y. Kobayashi, I. Terao, A. Mineshige, D. Urushihara, T. Asaka and K. Fukuda, *Solid State Ion.*, 2023, **399**, 116309.
14 K. Kobayashi, K. Hirai, T. Uchikoshi, Y. Sakka, T. Akashi and T. S. Suzuki, *Open Ceram.*, 2021, **6**, 100100.
15 K. Momma and F. Izumi, *J. Appl. Crystallogr.*, 2011, **44**, 1272–1276.
16 H. Okudera, Y. Masubuchi, S. Kikkawa and A. Yoshiasa, *Solid State Ion.*, 2005, **176**, 1473–1478.
17 S. Yan, D. Yang, S. Chen, J. Wen, W. He, S. Ji, Y. Xia, Y. Wang, L. Zhou and Y. Li, *Dalton Trans.*, 2020, **49**, 2578–2588.
18 K. Fujii, M. Yashima, K. Hibino, M. Shiraiwa, K. Fukuda, S. Nakayama, N. Ishizawa, T. Hanashima and T. Ohhara, *J. Mater. Chem. A*, 2018, **6**, 10835–10846.
19 N. Nunotani, N. Moriyama, K. Matsuo and N. Imanaka, *J. Ceram. Soc. Jpn.*, 2017, **125**, 773–775.
20 K. Matsuo, N. Nunotani and N. Imanaka, *J. Asian Ceram. Soc.*, 2021, **9**, 1466–1472.
21 P. K. Pandis, D. E. Perros and V. N. Stathopoulos, *Catal. Commun.*, 2018, **114**, 98–103.
22 K. Fukuda, T. Iwata and E. Champion, *Powder Diffr.*, 2006, **21**, 300–303.
23 J. E. H. Sansom, E. Kendrick, J. R. Tolchard, M. S. Islam and P. R. Slater, *J. Solid State Electrochem.*, 2006, **10**, 562–568.
24 H. Li, T. Baikie, S. S. Pramana, J. F. Shin, P. J. Keenan, P. R. Slater, F. Brink, J. Hester, T. An and T. J. White, *Inorg. Chem.*, 2014, **53**, 4803–4812.
25 S. Rehman, H. Kim, M. F. Khan, J. H. Hur, A. D. Lee and D. K. Kim, *Sci. Rep.*, 2019, **9**, 19387.
26 K. T. de C. Roseno, M. Schmal, R. Brackmann, R. M. B. Alves and R. Giudici, *Int. J. Hydrogen Energy*, 2019, **44**, 8166–8177.
27 J. C. Jung, H. Lee, H. Kim, Y. M. Chung, T. J. Kim, S. J. Lee, S. H. Oh, Y. S. Kim and I. K. Song, *Catal. Commun.*, 2008, **9**, 943–949.
28 J. C. Jung, H. Lee, H. Kim, Y. M. Chung, T. J. Kim, S. J. Lee, S. H. Oh, Y. S. Kim and I. K. Song, *Catal. Lett.*, 2008, **124**, 262–267.
29 A. Matsuda, H. Tateno, K. Kamata and M. Hara, *Catal. Sci. Technol.*, 2021, **11**, 6987–6998.
30 A. Matsuda, K. Obara, A. Ishikawa, M. H. Tsai, C. H. Wang, Y. C. Lin, M. Hara and K. Kamata, *Catal. Sci. Technol.*, 2023, **13**, 5180–5189.
31 J. Tian, J. Tan, Z. Zhang, P. Han, M. Yin, S. Wan, J. Lin, S. Wang and Y. Wang, *Nat. Commun.*, 2020, **11**, 5693.
32 P. Han, R. Yan, Y. Wei, L. Li, J. Luo, Y. Pan, B. Wang, J. Lin, S. Wan, H. Xiong, Y. Wang and S. Wang, *J. Am. Chem. Soc.*, 2023, **145**, 10564–10575.
33 K. Murata, K. Arai, N. Kondo, R. Manabe, T. Yumura and S. Hosokawa, *Catal. Sci. Technol.*, 2024, **14**, 3253–3264.
34 M. C. J. Bradford and M. A. Vannice, *Appl. Catal., A*, 1996, **142**, 73–96.
35 A. Oda, R. Ichihashi, Y. Yamamoto, K. Sawabe and A. Satsuma, *J. Mater. Chem. A*, 2023, **11**, 23854–23866.
36 K. C. Westaway, *J. Labelled Compd. Radiopharm.*, 2007, **50**, 989–1005.
37 C. Elmasides, T. Ioannides and X. E. Verykios, *AIChE J.*, 2000, **46**, 1260–1270.
38 A. G. Steghuis, J. G. Van Ommen and J. A. Lercher, *Catal. Today*, 1998, **46**, 91–97.
39 J. Zhu, J. G. Van Ommen and L. Lefferts, *J. Catal.*, 2004, **225**, 388–397.
40 Z. Ding, S. Chen, T. Yang, Z. Sheng, X. Zhang, C. Pei, D. Fu, Z. J. Zhao and J. Gong, *Nat. Commun.*, 2024, **15**, 4636.

